



An artificial intelligence based-model for heat transfer modeling of 5G smart poles

A. Khosravi ^{*}, T. Laukkanen, K. Saari, V. Vuorinen

Department of Mechanical Engineering, School of Engineering, Aalto University, Helsinki, Finland



ARTICLE INFO

Keywords:

5G smart pole
Heat transfer modeling
Artificial intelligence
Waste heat
ANFIS

ABSTRACT

The LuxTurrim5G project is built on integrating different types of sensors and equipment that have been integrated into light poles in order to build new data-driven services. One additional service could be to harvest the waste heat produced in the electrical devices in the pole. In this research, we developed an intelligent model for heat transfer modeling of 5G Smart Poles. The input parameters used to construct the model are latitude of the station (deg), ambient temperature ($^{\circ}\text{C}$), inside airflow (m^3/min) and time (h). These input parameters are employed to predict heat flow (W) and maximum plate temperature ($^{\circ}\text{C}$) inside the utility box. The results show that the ANFIS-PSO model provides an accurate prediction of R-value >0.95 for the test data, which is close to the maximum theoretically value of 1. The results showed that for the small amount of latitude, the maximum heat flow and temperature of the inside air is not detected at noon and the radiation heat flow to the vertical cylinder is maximized between sunrise and noon as well as between noon and sunset. The model also demonstrated that for the northern conditions, the temperature levels of heat generated over 30°C are limited.

1. Introduction

One of the biggest challenges of our society is facing global warming. It causes storms and intense drought, rising sea levels, melting glaciers, and warming oceans which directly jeopardize the animals' life and also it has many other adverse effects. In the United Nations Paris Climate Agreement humanity is globally seeking to limit greenhouse gas emissions to the atmosphere to a level that would limit the rise of atmospheric temperature to 1.5° [1]. On the other hand, the population expanding rises the demand for energy, food, and raw materials continuously straining the finite resources of the planet. Some developed countries have committed to even stricter emission limits and find alternatives for energy resources. As an example, Finland will try to be carbon neutral by 2035 [2]. This requires a considerable transformation in the transportation, industry, power and heating sectors.

This has a huge effect especially on future energy systems. Renewable energy sources (such as wind, solar, tidal, geothermal, hydro and biomass) will be the backbone of the future energy system [3], but additionally nuclear energy [4] and energy efficiency [5] will play a vital role. Most of these energy sources produce electricity directly, which in general will make future energy systems electrified [6]. The major drawback of most of these energy sources is that they are intermittent by nature and thus their production is more uncontrollable than traditional energy sources. For this reason, also energy storage [7] and consumption flexibility [8] will become major contributors to future energy systems.

* Corresponding author.

E-mail address: ali.khosravi@aalto.fi (A. Khosravi).

Nomenclature

A	Heat transfer area (m ²)
R	correlation coefficient
D	cylindrical vertical utility box diameter (m)
RMSE	root mean square error
D_h	hydraulic diameter inside the utility box (m)
S	wetted surface area (m ²)
G	Heat transfer conductance (W)
T	temperature (°C)
h	Heat transfer coefficient (W/m ² K)
Vmax	utility box cylinder volume (m ³)
K	conductance heat transfer coefficient (W/m.K)
z	zenith angle (°)
L	length of cylindrical vertical utility box (m)
ϵ	emissivity
\bar{Nu}	average Nusselt number
τ	transmittance of the atmosphere
Pr	Prandtl number
α	Sun elevation angle (°)
Q''_n	total radiation power (W/m ²)
φ_1	sun radiation (W/m ²)
Re	Reynolds number

In Nordic countries heating of buildings in cold seasons is one major contributor to energy needs. Traditionally, heating has been based on the burning of wood inland and on gas and coal in coastal areas. Especially in urban areas, the heat has been produced in centralized and energy-efficient combined heat and power (CHP) plants where the heat has been transferred to customers by district heating pipelines. However, the use of fossil fuels, especially coal, will decrease in order to make cities carbon neutral. For example, in Finland, coal will be banned as a source of energy generation during 2029 [9]. Thus, the major options in district heating are to increase the usage of biomass or to also electrify district heating (DH), which can be done by using electricity directly or more efficiently with heat pumps. However, in addition to electricity, heat pumps also need a heat source that should have high as possible temperature and, above all, this heat should be very cheap for energy- and cost-efficient operation. Thus, different sources of waste heat play an important role in the future as does the sectoral integration of heat and power generation [10]. In heating, energy storage solutions and consumption elasticities will become more important [11]. The feasibility of waste heat recovery is determined by considering different internal agents that are quantity and quality of the heat source, the stream composition, the limitations for the stream temperature and external agents such as accessibility or economics. Studying altogether these parameters allows determining the better system to use according to each heat and stream source. Heat quantity is the whole amount of energy that can be harvested from a heat source; heat quality is the exergetic or useful part of the heat quantity; stream composition is related to the composition of the fluid, heat transfer coefficient and heat capacity; and minimum temperature allowed is related to the exchanger material limitations.

The major trends of digitalization and urbanization make urban environments play a key role in the transformation of sustainable energy systems. Cities will become smarter by collecting and monitoring data obtained with different types of sensors. This data can be used in optimizing the efficiency of city operations including the energy systems of the cities [12,13]. Thus, digitalization on one hand, and the pressure of intermittent renewable energy resources, on the other hand, force future urban areas to transform their energy systems. The goal of the LuxTurrim5G project [14] is to build new data-driven services by integrating data from different sensors embedded in the utility box of the 5G pole. One additional service could be to harvest the waste heat produced in the electrical devices in the pole and utilize this waste heat in a local energy system [15]. The heat generated by the electronic devices in the utility box also has an adverse effect on the data transfer capacity and efficiency of the system. So, harvesting the waste heat can increase the efficiency of the system as well as the lifetime of the electronic devices.

Waste heat energy harvesting from different low-temperature sources to be used in local energy systems and, especially in heating systems, are numerous, including studies and reviews related to industrial waste heat [16–19] and to low-temperature heat sources [20–22]. The only article where the low-temperature heat source is a 5G smart pole is [15], and in that article, the actual temperature level and heat amount possible to be recovered were approximated, while in this work these values are calculated.

On the other hand, to catch the hidden pattern between the input parameters and targets, in this research, we developed an intelligent model based on machine learning algorithms (MLAs). Many engineering problems have greatly benefited from the power of machine learning over the years [23–26]. And also, many salient methods of machine learning and artificial intelligence (AI) have been developed to prevail over the current challenges. Garud et al. [27] implemented an AI model to estimate the thermal efficiency of a thermoelectric generator for waste heat recovery. Their research showed that the employed AI model performed better than the coupled numerical approach. Herawan et al. [28] used AI to predict the waste heat energy recovery performance in a naturally aspirated engine. They investigated the effect of input parameters to increase the efficiency of the process and the AI model accurately

predicted the target. Hussein [29] implemented an adaptive neuro-fuzzy inference system (ANFIS) to predict the heat transfer coefficient and friction factor for a nanofluid flow. This model was improved by Khosravi et al. [30]. They developed different methods of MLAs to predict wind speed in Osorio wind farm, Brazil. It was concluded that hybrid methods such as ANFIS combined with evolutionary algorithms have better prediction performance compared to the other MLAs.

1.1. Objectives

In this article, the objective is to study how much, when and at what temperature level heat is obtained from 5G smart poles in different stations across the world. Based on this information, an intelligent model based on an adaptive neuro-fuzzy inference system optimized with particle swarm optimization (ANFIS-PSO) is implemented. The model can directly be integrated into models of local energy systems for studying the possibilities to harvest heat from 5G smart poles in different climatic conditions. Thus, the neural network model of the 5G smart pole can be integrated with other subsectors – or units (which can also be neural networks) of a local energy system.

2. Material and methods

2.1. Heat transfer model of the utility box

Heat balance is calculated on three different surfaces of the cylindrical utility box. Surface 1 is the sun radiation side of the cylinder, surface 2 is the electrically heated plate within the cylinder and surface 3 is the shadow side of the cylinder. The notation and simplified picture of the system can be seen in Fig. 1.

Sun radiation side surface is calculated by:

$$\varphi_1 + (T_2 - T_1)G_{r1} = (T_1 - T_{amb})G_0 + (T_1 - T_{in})G_1 \quad (1)$$

where φ_1 is sun radiation heat flow.

Electrically heated plate inside of the cylinder is:

$$\varphi_2 = (T_2 - T_{in})G_2 + (T_2 - T_1)G_{r1} + (T_2 - T_3)G_{r3} \quad (2)$$

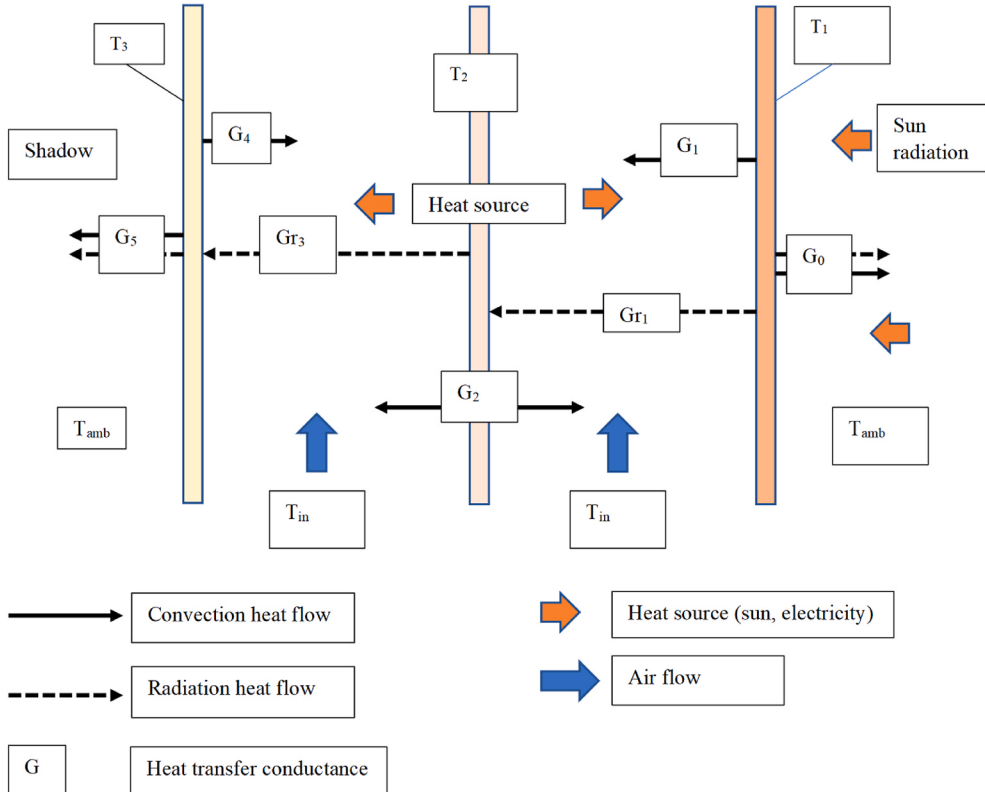


Fig. 1. Heat transfer model of the utility box.

where φ_2 is electric heating heat flow.

Shadow side surface is calculated by the following equation.

$$(T_2 - T_3)G_{r3} = (T_3 - T_{amb})G_5 + (T_3 - T_{in})G_4 \quad (3)$$

The heat transfer conductance G is defined as

$$G = KA \quad (4)$$

where K is heat transfer coefficient and A is corresponding heat transfer area.

2.1.1. Radiation heat transfer models

The total radiation power Q''_n [W/m²] of sun hitting normal to a surface A can be calculated as [16].

$$Q''_n = Q''_0 \tau^m \quad (5)$$

where $Q''_0 = 1395$ W/m² and τ is the transmittance of the atmosphere ($\tau = 0, 75$). The parameter m is

$$m = \frac{1}{\cos z} \quad (6)$$

where z is zenith angle. Sun elevation angle α is given as:

$$\alpha = 90^\circ - z \quad (7)$$

The radiation power of sun hitting the projected area of cylindrical vertical utility box with a diameter D and length L is calculated based on emissivity $\epsilon = 0.8$, elevation angle α and Lambert's cosine law

$$\Phi = \epsilon L D \cos(\alpha) Q''_n \quad (8)$$

Radiation heat transfer between cylinder surfaces and plate within the cylinder as well as between cylinder surfaces and ambient is calculated based on black body radiation between surfaces, which is corrected using the approximated emissivity of 0.8.

2.1.2. Convection heat transfer models

Convection heat transfer of inside airflow is calculated assuming laminar flow and simultaneously developing thermal and flow boundary layers. The average Nusselt number is [17].

$$\overline{Nu} = \frac{0.664}{0.95\sqrt{X}} \sqrt{1 + 7.3(0.95X)^{0.5}} \quad (9)$$

$$X = \frac{H}{D_h Re Pr} \quad (10)$$

The effective length of the developing boundary layer is assumed to be $H = 0.2$ m, which is the approximated length of electronic components inside the utility box. The average hydraulic diameter inside the utility box is based on free volume V and wetted surface S . The free volume of the utility box is estimated to be 56% of the maximum cylinder volume, when

$$D_h = \frac{4V}{S} = \frac{4 * 0.56 V_{max}}{S} = 0.096m \quad (11)$$

Here V_{max} corresponds to empty utility box cylinder volume and wetted surface area S is calculated based on cylinder surface area added by the surface area of the inside plate.

The average inside air velocity and Reynolds number is calculated assuming that only 56% of the maximum cross-sectional flow area is free for flow:

$$A = 0.56 A_{max} = 0.56 \frac{\pi D^2}{4} = 0.044 m^2 \quad (12)$$

The convection heat transfer coefficient outside of the cylindrical utility box is calculated assuming that wind velocity $U = 0$. The heat transfer coefficient h of natural convection on a vertical wall is calculated using a dimensional equation which is based on the temperature difference between wall and air [17].

$$h = 2.2(\Delta T)^{0.25} \quad (13)$$

The used dimensions are h [W/m²K] and T [K].

2.1.3. Calculation procedure

The cylindrical utility box with a diameter of $D = 0.315$ m and length $L = 2.5$ m is divided into 5 different sections with a length of 0.5 m. For the first section, the ambient air temperature T_{amb} is the inlet temperature of the cooling air ($T_{in} = T_{amb}$). The sun radiation

power is calculated using Eq. (5) and the electrical heating of the plate inside is calculated. The surface temperatures T_1 , T_2 and T_3 for the first section are solved using Eqs. (1-3). Then based on the convective conductance G_1 , G_2 and G_4 and the surface temperatures, the air temperature rise in the first section and the new air inside temperature is calculated. This temperature is then used as an inlet temperature for the second section. The calculation is then repeated up to the outlet of the cooling air.

This way both the surface temperatures T_1 , T_2 and T_3 and the heat flow to the cooling air can be calculated at 5 different locations. The values at the outlet can be used to calculate the overall heat flow to the air and maximum surface temperatures.

2.2. ANFIS-PSO model

Each fuzzy system composes three main parts including fuzzification, inference engine and defuzzification. Knowledge of human expert is applied to adjust the structure of a fuzzy logic system [31]. To obtain this ability automatically, artificial neural networks (ANNs) are applied as a combination with the fuzzy system, which the new system is called neuro-fuzzy system. Mamdani and Sugeo-Takaki are two types of fuzzy systems, which Sugeno-Takaki type is employed in this study for developing an ANFIS system because this type of fuzzy model works well with optimization and adaptive techniques [32].

A simple structure of an ANFIS with two inputs and one output is illustrated in Fig. 2. The rules base contains two Sugeno “if-then” rules that are defined by Eqs. (14) and (15) as follows:

Rule 1:

$$\text{If } x \text{ is } A_1 \text{ and } y \text{ is } B_1, \text{ then } f_1 = p_1x + q_1y + r_1 \quad (14)$$

Rule 2:

$$\text{If } x \text{ is } A_2 \text{ and } y \text{ is } B_2, \text{ then } f_2 = p_2x + q_2y + r_2 \quad (15)$$

It could be plainly viewed that an ANFIS model contains five layers, which are fuzzification, rule, normalization, defuzzification and sum layer. In this study, we developed an intelligent model by a combination of ANFIS and particle swarm optimization algorithm (PSO). PSO is a type of evolutionary algorithms that is employed to find the best solution to optimization problems. Indeed, PSO is applied to obtain the best fuzzy parameters, more details can be found in [33]. The structure of this model is formed by considering latitude of the station (deg), ambient temperature ($^{\circ}\text{C}$), inside airflow ($^{\circ}\text{C}$), wind speed (m/s) and time (h) as input parameters. The model uses the input parameters to predict the targets, which are heat flow (W) and maximum plate temperature ($^{\circ}\text{C}$) inside the utility box (metallic support plate) as presented in Fig. 3. A schematic diagram of the utility box is presented in Fig. 4.

The prediction performance of the intelligent method (ANFIS-PSO) is assessed with the statistical indicators (root mean square error (RMSE) and correlation coefficient (R)) as presented in Eqs. (16) and (17).

$$RMSE = \sqrt{\frac{1}{n} \sum_{i=1}^n (x_i - y_i)^2} \quad (16)$$

$$R = \frac{\sum_{i=1}^n (x_i - \bar{x})(y_i - \bar{y})}{\sqrt{\sum_{i=1}^n (x_i - \bar{x})^2 \sum_{i=1}^n (y_i - \bar{y})^2}} \quad (17)$$

where x_i , y_i , \bar{x} , \bar{y} and n are observed value, predicted value, mean of observed data, mean of predicted data and number of data, respectively. The number of data for each time interval is 3800.

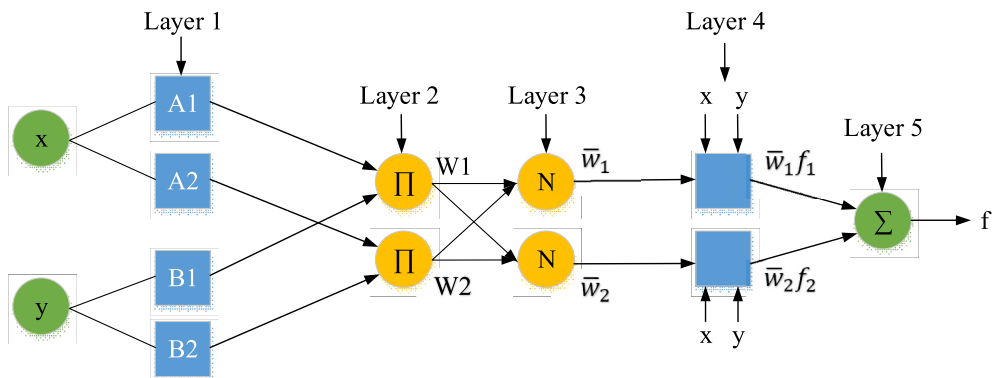


Fig. 2. A simple structure of an ANFIS model including five different layers.

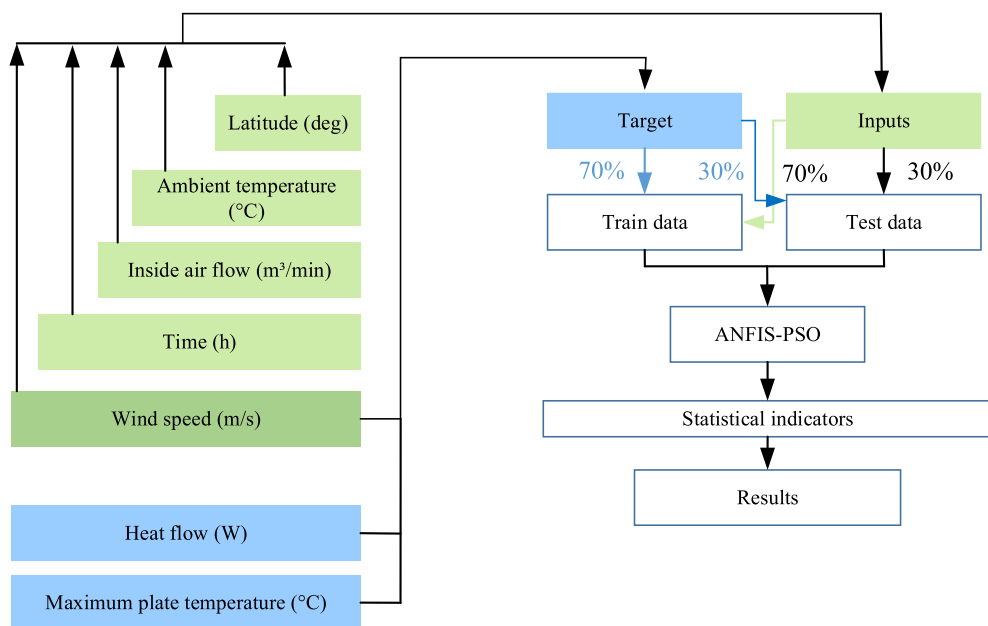


Fig. 3. Structure of the intelligent model for prediction of heat flow and maximum plate temperature.

SCHEMATIC UTILITY BOX

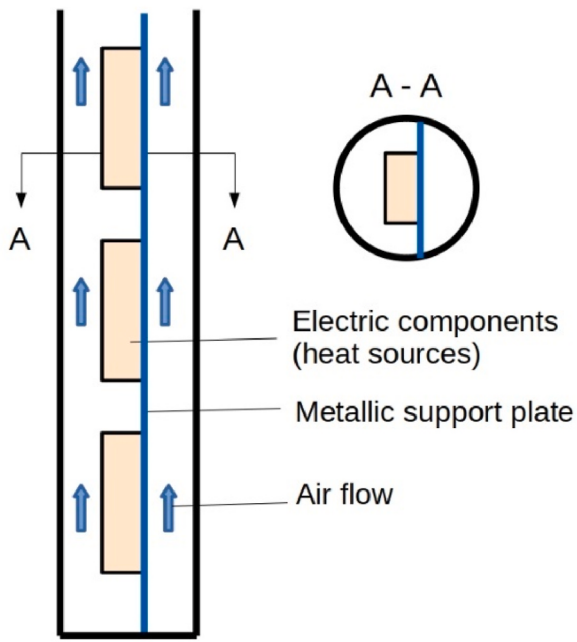


Fig. 4. Schematic diagram of the utility box.

3. Results and discussion

3.1. Heat transfer model

The maximum (= outlet) temperature of the inside air and the heat flow to the inside air are presented as contour plots for different latitudes for midsummer and September (also November for Helsinki). The latitudes correspond to Helsinki (60°), Rome (40°) and the

equator (0°). At midsummer, the assumed ambient temperatures are 25, 30 and 40 °C and at September 15, 20 and 40 °C. The x-axis is the inside airflow rate and y-axis the time of the day. The sky is assumed to be clear (no clouds) and the wind velocity is assumed to be 2 m/s which is almost calm. The ambient temperature is assumed to be constant during the day and night in all calculations. It is also assumed that the transients are so slow that heat capacities can be ignored.

The results show that when the latitude is small, the maximum heat flow and temperature of the inside air are not detected at noon, but forenoon and afternoon. The Lambert's cosine law of radiation should give the maximum values for the solar radiation hitting the

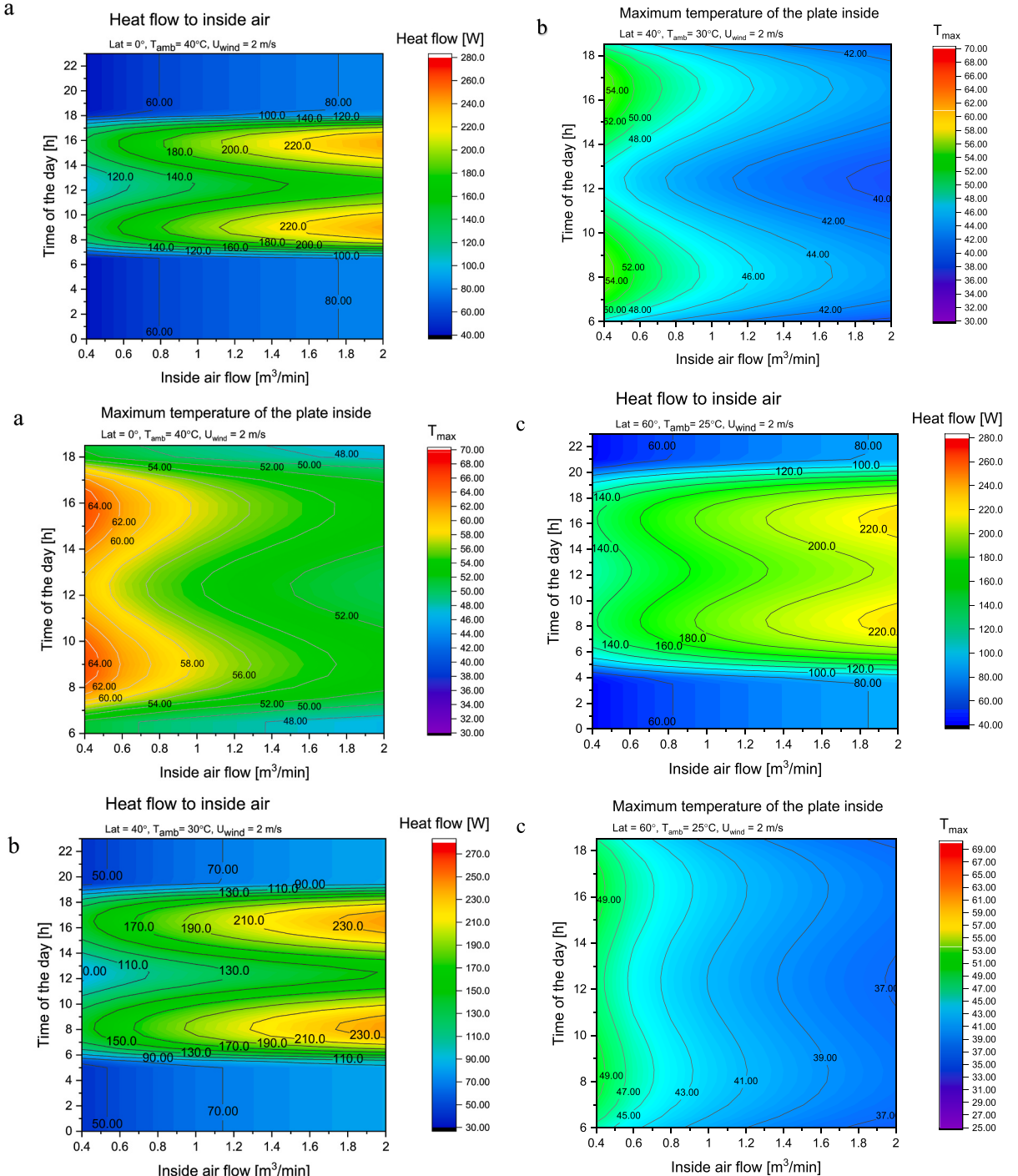


Fig. 5. a), Heat flow (W) and maximum plate temperature (°C) for Africa at midsummer, b) Heat flow (W) and maximum plate temperature (°C) for Rome at midsummer, c) Heat flow (W) and maximum plate temperature (°C) for Helsinki at midsummer.

vertical cylinder, when the sun is rising up or setting down. However, according to Eqs. (5), (6) and (7) the solar radiation through the atmosphere is diminished by the adsorption of air molecules when the elevation angle is small. When the elevation angle increases, the adsorption is decreasing, and Lambert's cosine law begins to dominate the radiation heat flow. This means that when the latitude is small, the radiation heat flow to the vertical cylinder is actually maximized somewhere between sunrise and noon and also between noon and sunset. You can easily see heat flow and temperature peaks at 9 and 16 o'clock in Fig. 5(a–c). This behavior is flattened when

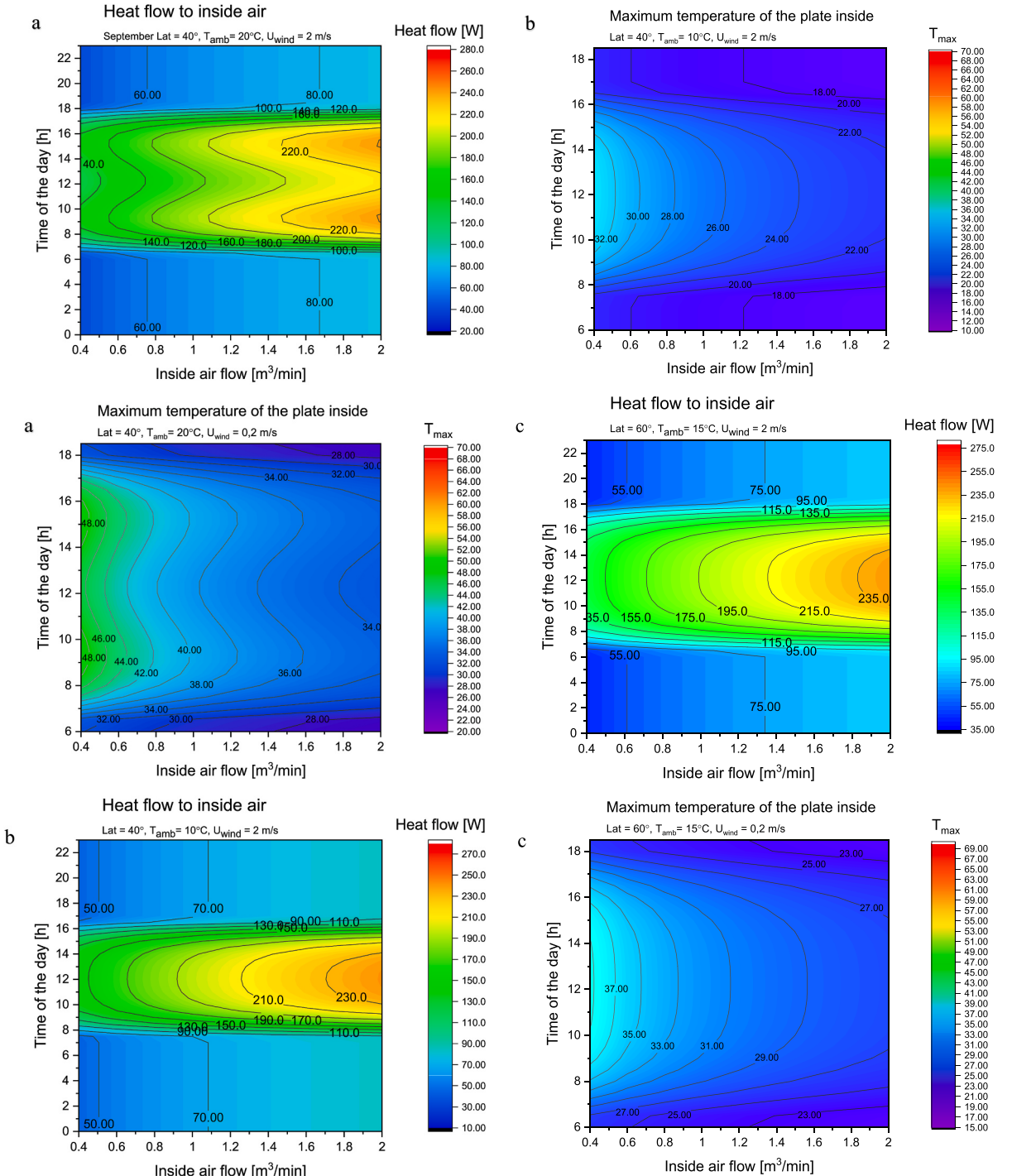


Fig. 6. a) Heat flow (W) and maximum plate temperature (°C) for Rome in September, b) Heat flow (W) and maximum plate temperature (°C) for Helsinki in September, c) Heat flow (W) and maximum plate temperature (°C) for Rome in November, d) Heat flow (W) and maximum plate temperature (°C) for Helsinki in November.

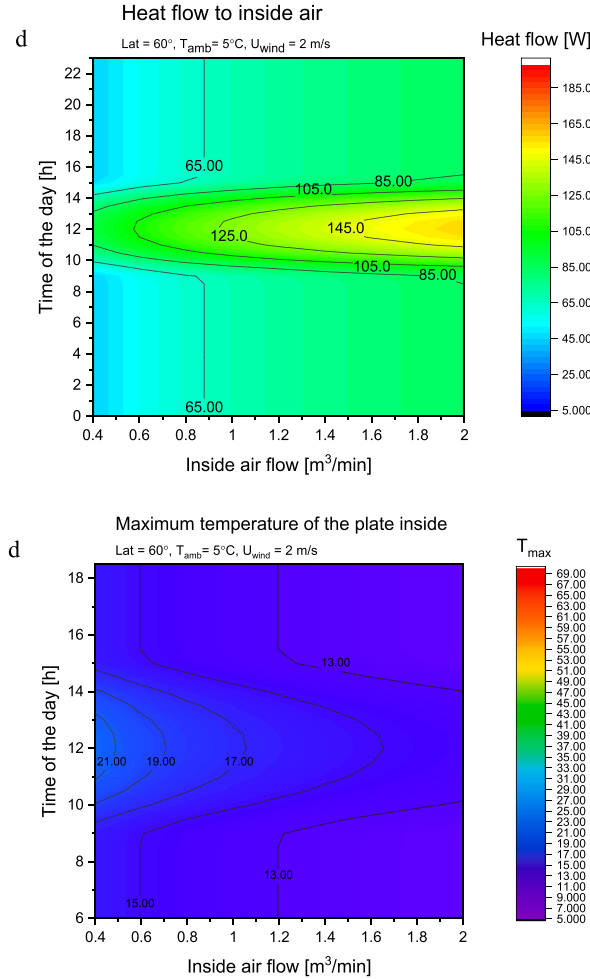


Fig. 6. (continued).

the latitude is increased and even more in wintertime, when the sun elevation angle is small during the whole day. In wintertime, the solar radiation hitting the vertical cylinder does not have any more two peaks, but the radiation profile is flattened to one peak profile, which is seen also in heat flow and temperature profiles in Fig. 6(a–d).

3.2. ANFIS-PSO model

Three different scenarios were defined and investigated to predict the targets, as presented in Table 1. ANFIS-PSO model was trained with the input parameters designated in S1, S2 and S3. The number of clusters for training the network was 20. Also, for PSO parameters the maximum iteration and number of populations were adjusted to be 500, and the personal learning coefficient and global learning coefficient were 1 and 2, respectively. We also trained the network for midsummer, September and November.

Table 2 summarizes the prediction accuracy of the ANFIS-PSO model for estimating heat flow and maximum plate temperature for S1, S2 and S3. Clearly from the table, it can be concluded that S3 outperforms S1 and S2. It shows considering the time (h) as input parameter can significantly increase the performance prediction of the model, as can be observed for heat flow, $R_{test,S1} = 0.397$, $R_{test,S2} = 0.413$, and $R_{test,S3} = 0.954$, and for maximum plate temperature, $R_{test,S1} = 0.135$, $R_{test,S2} = 0.089$, and $R_{test,S3} = 0.993$.

Table 1
Three different scenarios for input parameters to train the ANFIS-PSO model.

Scenario	Inputs
S1	latitude (deg), T _{amb} (°C), Inside airflow (m ³ /min)
S2	latitude (deg), T _{amb} (°C), Inside airflow (m ³ /min), Wind speed (m/s)
S3	latitude (deg), T _{amb} (°C), Inside airflow (m ³ /min), Wind speed (m/s), Time (h)

Table 2

Statistical indicators for predicting heat flow and maximum plate temperature by considering three different scenarios as input.

Inputs	Target	Train		Test	
		R	RMSE	R	RMSE
S1	Heat Flow (W)	0.366	54.33	0.397	54.91
S2	Heat Flow (W)	0.438	52.75	0.413	53.57
S3	Heat Flow (W)	0.953	17.65	0.954	17.70
S1	Maximum plate temperature (°C)	0.137	23.68	0.135	24.14
S2	Maximum plate temperature (°C)	0.166	23.74	0.089	23.86
S3	Maximum plate temperature (°C)	0.995	2.312	0.993	2.649

Fig. 7 illustrates the training and testing phase of the ANFIS-PSO model for predicting the heat flow. As can be observed from the figure, the model can precisely predict the target as outputs relatively accurately follow the targets. This shows the model has been successfully trained and it can precisely predict the target in the testing phase. Also, the training and testing phases of the model for the prediction of the maximum plate temperature are illustrated in Fig. 8.

The intelligent model catches the hidden pattern between the input parameters and target. This is a kind of supervised learning in which we train the model with datasets to predict outcomes accurately. As an example, Fig. 9 demonstrates the ANFIS-PSO decision surfaces to predict the heat flow-S3. These figures obviously show how the intelligent model can predict the heat flow using input

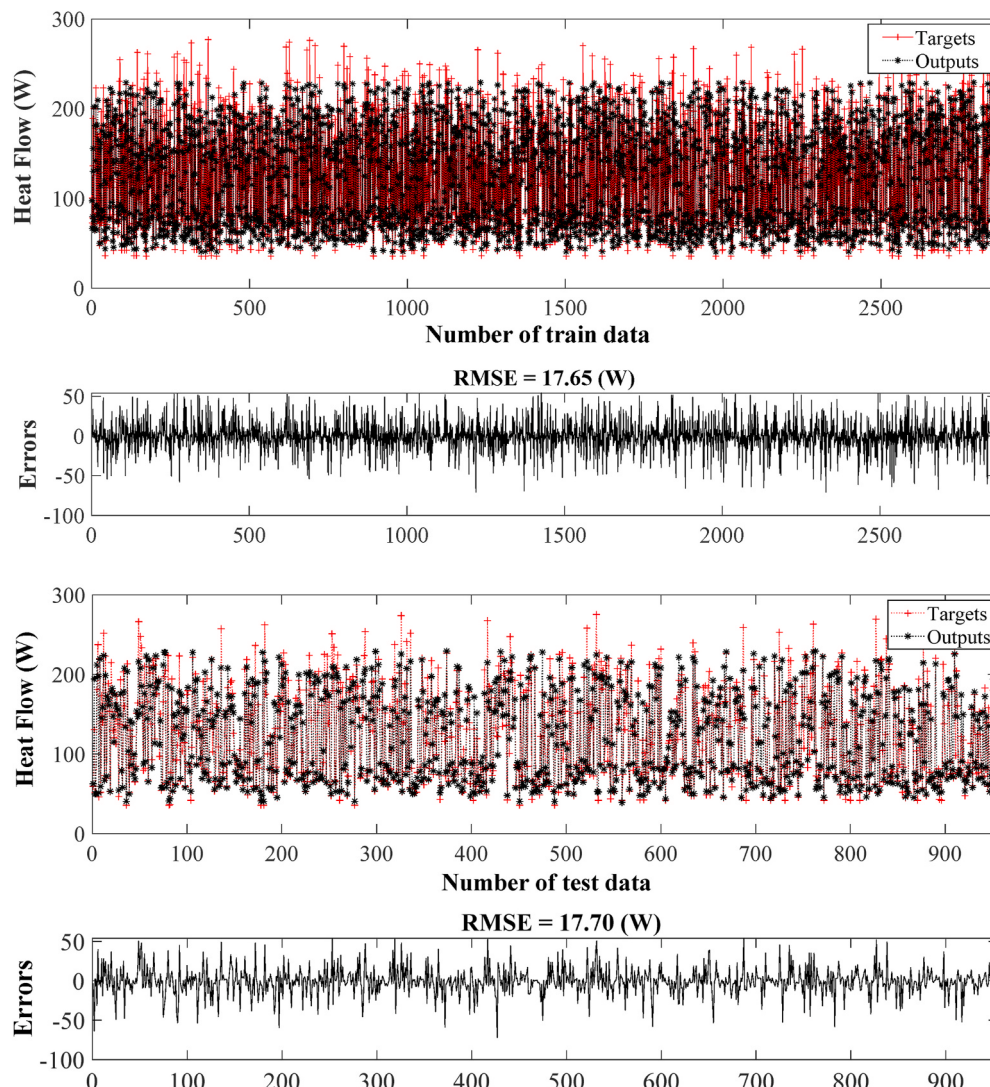


Fig. 7. Training and testing phases of the ANFIS-PSO model for predicting heat flow-S3.

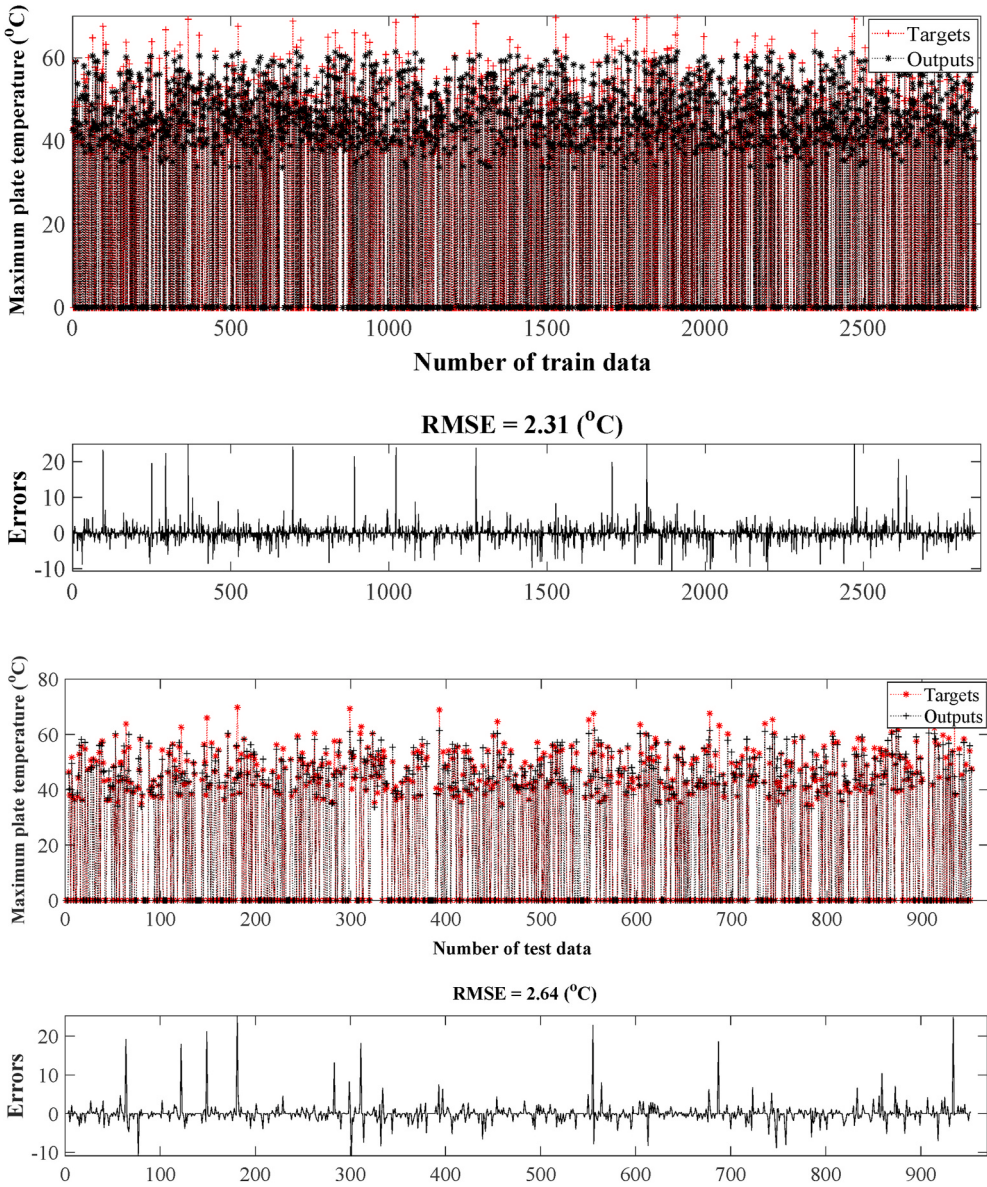


Fig. 8. Training and testing phases of the ANFIS-PSO model for predicting maximum plate temperature-S3.

parameters. Heat flow has a tendency to increase by increasing the ambient temperature and decreasing the latitude of the station as can be observed in Fig. 9-a. By decreasing the wind speed and increasing the inside airflow, the heat flow increases, Fig. 9-b. Moreover, the model completely extracted the role of time to predict the heat flow as can be seen in Fig. 9-c.

Tables 3 and 4 also present the prediction performance of the model for predicting the heat flow and maximum plate temperature for September and November, respectively. In the same way, we trained the network by three different scenarios for each target. It is grasped from the results that considering the time as an input parameter would significantly improve the prediction performance for heat flow and maximum plate temperature. R-values higher than 0.98 show the model can successfully predict the targets. For September, considering input parameters as presented in S3, the model predicts the heat flow with R and RMSE of 0.991 and 8.225 W for test data, respectively. In addition, for November, the maximum plate temperature was predicted by the model with R and RMSE values of 0.984 and 2.851, respectively.

4. Conclusion

5G smart poles are devices that integrate many kinds of equipment including antennas, base stations, sensors, displays, street lightning and other devices that provide services for smart cities. These electric devices also need electricity, and generate heat. This

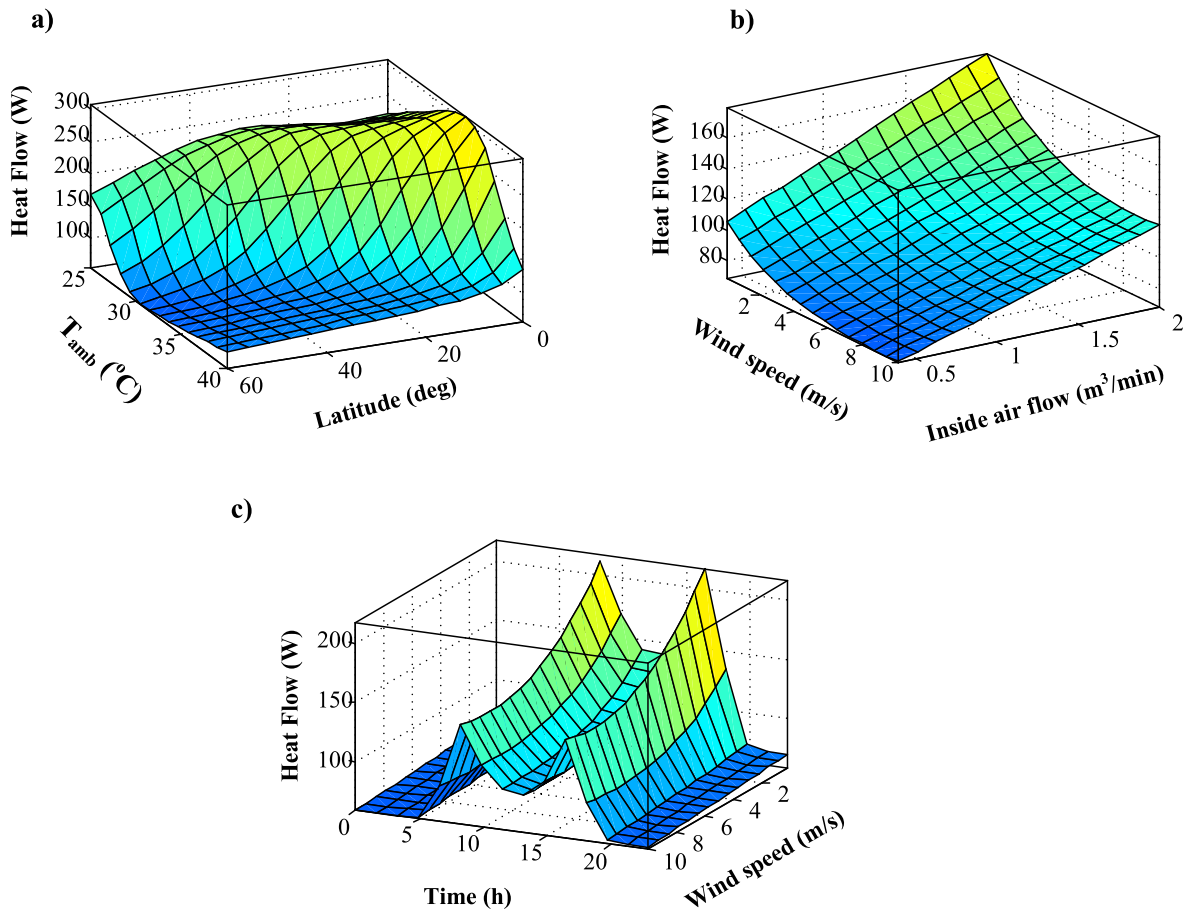


Fig. 9. ANFIS-PSO decision surfaces for heat flow prediction.

Table 3

Performance prediction of the ANFIS-PSO model for predicting the heat flow and maximum plate temperature, results for September.

Inputs	Target	Train		Test	
		R	RMSE	R	RMSE
S1	Heat Flow (W)	0.300	60.36	0.2941	61.37
S2	Heat Flow (W)	0.3994	57.94	0.3622	60.133
S3	Heat Flow (W)	0.9916	8.2257	0.9916	8.1177
S1	Maximum plate temperature ($^{\circ}$ C)	0.1429	16.0995	0.0851	16.2614
S2	Maximum plate temperature ($^{\circ}$ C)	0.153	16.0839	0.0847	16.2568
S3	Maximum plate temperature ($^{\circ}$ C)	0.9867	2.6429	0.9847	2.8517

Table 4

Performance prediction of the ANFIS-PSO model for predicting the heat flow and maximum plate temperature, results for November.

Inputs	Target	Train		Test	
		R	RMSE	R	RMSE
S1	Heat Flow (W)	0.4354	42.42	0.4552	44.31
S2	Heat Flow (W)	0.5114	41.09	0.4462	42.78
S3	Heat Flow (W)	0.9806	9.2855	0.9823	9.2668
S1	Maximum plate temperature ($^{\circ}$ C)	0.2516	9.7767	0.2634	9.6664
S2	Maximum plate temperature ($^{\circ}$ C)	0.2643	9.6721	0.2012	10.04
S3	Maximum plate temperature ($^{\circ}$ C)	0.9782	2.0849	0.9801	2.0324

study proposes an intelligent model based on ANFIS-PSO to simulate the heat transfer modeling of a 5G Smart pole. This model is used to calculate the maximum temperature of the plate inside the utility box and heat flow in such 5G smart poles with varying values of input parameters (airflow velocity inside the pole, latitude, ambient temperature, wind speed and time of the day). This model and the information that it provides can be used to calculate the heat amount available to be used as a waste heat source for a local energy system and easily integrated with other subprocesses of models of the local energy system.

The data needed for the neural network is provided with a detailed simulation model that calculates the heat flows in the pole with varying environmental conditions and the amount of airflow inside the pole. The results showed that heat flow and temperature inside the utility box are not detected at noon, for small amounts of latitude. In addition, the radiation heat flow to the vertical cylinder was maximized between sunrise and noon and also somewhere between noon and sunset (peak values were observed at 9 and 16 o'clock). But the pattern is changed when the latitude is increased as well as in wintertime. This is due to decreasing the sun elevation angle during the whole day. So, in wintertime, the solar radiation on the vertical cylinder just has one peak profile.

Based on these simulations and the intelligent model, the amount of heat at temperature levels over 30 °C are limited in northern conditions especially in the winter, when the need for heating is most needed. Additionally, it is evident that in latitudes close to the equator temperature of the air inside the pole can rise to such high levels, which can harm the sensitive electrical devices inside the pole. So, for these regions, we suggest using a cooling system for 5G Smart poles to prevent damage to electronic devices.

Three different scenarios are developed to assess the role of input parameters to predict the targets in the intelligent model. It is evident that the scenario also considering the time of the day as an input is the best providing R-values >0.95, which are very close to the theoretically best possible value of 1. Thus, a very accurate model is provided.

CRediT statements

Ali Khosravi: Conceptualization, Data gathering, Investigation, Methods, Software, Writing- Original draft preparation, Validation, Visualization. Timo Laukkanen: Conceptualization, Methods, Validation, Data gathering, Visualization, Reviewing and Editing. Kari Saari: Conceptualization, Visualization, Methods, Software, Writing- Reviewing and Editing. Ville Vuorinen: Conceptualization, Methods, Supervision, Visualization, Funding acquisition, Reviewing and Editing.

Declaration of competing interest

The authors declare that they have no known competing financial interests or personal relationships that could have appeared to influence the work reported in this paper.

Acknowledgement

The authors would like to acknowledge Business Finland for their financial support for the LuxTurrim5G project. We also acknowledge Aalto University, Department of Mechanical Engineering, for the support of the project.

References

- [1] D.S. Cocco, A.M.S. Costa, Effect of a global warming model on the energetic performance of a typical solar photovoltaic system, *Case Stud. Therm. Eng.* 14 (Sep. 2019) 100450.
- [2] Government's climate policy: carbon neutral Finland 2035 - Ympäristöministeriö [Online], <https://ym.fi/en/carbon-neutral-finland-2035>. (Accessed 1 April 2021).
- [3] H. Lund et al., "Renewable Energy Systems A Smart Energy Systems Approach to the Choice and Modeling of 100% Renewable Solutions Second Edition".
- [4] B. van der Zwaan, The role of nuclear power in mitigating emissions from electricity generation, *Energy Strateg. Rev.* 1 (4) (May 2013) 296–301.
- [5] M. Ringel, B. Scholmann, M. Kral, C. Rohde, Towards a green economy in Germany? The role of energy efficiency policies, *Appl. Energy* 179 (Oct. 2016) 1293–1303.
- [6] J.A. De Chalendar, P.W. Glynn, S.M. Benson, City-scale decarbonization experiments with integrated energy systems, *Energy Environ. Sci.* 12 (5) (May 2019) 1695–1707.
- [7] P.E. Dodds, S.D. Garvey, The role of energy storage in low-carbon energy systems, in: *Storing Energy: with Special Reference to Renewable Energy Sources*, Elsevier Inc., 2016, pp. 3–22.
- [8] P. Palensky, D. Dietrich, Demand side management: demand response, intelligent energy systems, and smart loads, *IEEE Trans. Ind. Informatics* 7 (3) (Aug. 2011) 381–388.
- [9] The act banning the use of coal for energy generation in 2029 to enter into force in early April [Online], <https://valtioneuvosto.fi/en/-/1410877/kivihiilen-energiakayton-vuonna-2029-kieltava-laki-voimaan-huhtikuun-alussa>. (Accessed 1 April 2021).
- [10] F. Wang, et al., Thermodynamic analysis of solid oxide electrolyzer integration with engine waste heat recovery for hydrogen production, *Case Stud. Therm. Eng.* 27 (Oct. 2021) 101240.
- [11] L. Liu, J. Li, J. Niu, J.Y. Wu, Evaluation of the energy storage performance of PCM nano-emulsion in a small tubular heat exchanger, *Case Stud. Therm. Eng.* 26 (Aug. 2021) 101156.
- [12] B.N. Silva, M. Khan, K. Han, Towards sustainable smart cities: a review of trends, architectures, components, and open challenges in smart cities, *Elsevier Ltd, Sustainable Cities and Society* 38 (01-Apr-2018) 697–713.
- [13] K.T. Chui, M.D. Lytras, A. Visvizi, Energy sustainability in smart cities: artificial intelligence, smart monitoring, and optimization of energy consumption, *Energies* 11 (11) (Oct. 2018) 2869.
- [14] LuxTurrim5G ecosystem builds the smart city of the future — LuxTurrim5G." [Online]. Available: <https://www.luxturrim5g.com/new-blog/2019/5/28/luxturrim5g-ecosystem-builds-the-smart-city-of-the-future>. [Accessed: 20-Jan-2020].
- [15] A. Khosravi, T. Laukkanen, V. Vuorinen, S. Syri, Waste heat recovery from a data centre and 5G smart poles for low-temperature district heating network, *Energy* 218 (Mar. 2021) 119468.
- [16] S. Brückner, S. Liu, L. Miró, M. Radspieler, L.F. Cabeza, E. Lävemann, Industrial waste heat recovery technologies: an economic analysis of heat transformation technologies, *Appl. Energy* 151 (Aug. 2015) 157–167.

- [17] H. Lu, L. Price, Q. Zhang, Capturing the invisible resource: analysis of waste heat potential in Chinese industry, *Appl. Energy* 161 (Jan. 2016) 497–511.
- [18] R. Agathokleous, et al., Waste heat recovery in the EU industry and proposed new technologies, in: *Energy Procedia*, vol. 161, 2019, pp. 489–496.
- [19] D. Brough, H. Jouhara, The aluminium industry: a review on state-of-the-art technologies, environmental impacts and possibilities for waste heat recovery, Elsevier B.V. *International Journal of Thermofluids* 1–2 (01-Feb-2020) 100007.
- [20] A. Omar, M. Saghafifar, K. Mohammadi, A. Alashkar, M. Gadalla, A review of unconventional bottoming cycles for waste heat recovery: Part II – Applications, Elsevier Ltd, *Energy Convers. Manag.* 180 (15-Jan-2019) 559–583.
- [21] K. Ebrahimi, G.F. Jones, A.S. Fleischer, A review of data center cooling technology, operating conditions and the corresponding low-grade waste heat recovery opportunities, Elsevier Ltd, *Renew. Sustain. Energy Rev.* 31 (01-Mar-2014) 622–638.
- [22] D.M. van de Bor, C.A. Infante Ferreira, A.A. Kiss, Low grade waste heat recovery using heat pumps and power cycles, *Energy* 89 (Sep. 2015) 864–873.
- [23] P. Naphon, T. Arisaryawong, S. Wiriyasart, A. Srichat, ANFIS for analysis friction factor and Nusselt number of pulsating nanofluids flow in the fluted tube under magnetic field, *Case Stud. Therm. Eng.* 18 (Apr. 2020) 100605.
- [24] M. Ghalandari, M. Irandoost Shahrestani, A. Maleki, M. Safdari Shadloo, M. El Haj Assad, Applications of intelligent methods in various types of heat exchangers: a review, *J. Therm. Anal. Calorim.* 145 (4) (Aug. 2021) 1837–1848.
- [25] M. El Haj Assad, I. Mahariq, R. Ghandour, M.A. Nazari, T. Abdeljawad, Utilization of machine learning methods in modeling specific heat capacity of nanofluids, *Comput. Mater. Continua (CMC)* 70 (1) (2021) 361–374.
- [26] M.E.H. Assad, I. Mahariq, Z. Al Barakeh, M. Khasawneh, M.A. Amooie, Modeling CO₂emission of Middle Eastern countries using intelligent methods, *Comput. Mater. Continua (CMC)* 69 (3) (2021) 3767–3781.
- [27] K.S. Garud, J.-H. Seo, C.-P. Cho, M.-Y. Lee, Artificial neural network and adaptive neuro-fuzzy interface system modelling to predict thermal performances of thermoelectric generator for waste heat recovery, *Symmetry (Basel.)* 12 (2) (Feb. 2020) 259.
- [28] S. Gazali Herawan, A. Hakim Rohhaizan, A. Putra, A. Faris Ismail, Prediction of Waste Heat Energy Recovery Performance in a Naturally Aspirated Engine Using Artificial Neural Network, 2014.
- [29] A.M. Hussein, Adaptive Neuro-Fuzzy Inference System of friction factor and heat transfer nanofluid turbulent flow in a heated tube, *Case Stud. Therm. Eng.* 8 (Sep. 2016) 94–104.
- [30] A. Khosravi, L. Machado, R.N. Oliviera, Time-series prediction of wind speed using machine learning algorithms: a case study Osorio wind farm, Brazil, *Appl. Energy* 224 (C) (2018) 550–566.
- [31] A. Khosravi, R.N.N. Koury, L. Machado, J.J.G. Pabon, Prediction of wind speed and wind direction using artificial neural network, support vector regression and adaptive neuro-fuzzy inference system, *Sustain. Energy Technol. Assessments* 25 (Feb. 2018) 146–160.
- [32] A. Khosravi, R.O. Nunes, M.E.H. Assad, L. Machado, Comparison of artificial intelligence methods in estimation of daily global solar radiation, *J. Clean. Prod.* 194 (Sep. 2018) 342–358.
- [33] A. Khosravi, L. Machado, R.N. Oliviera, Time-series prediction of wind speed using machine learning algorithms: a case study Osorio wind farm, Brazil, *Appl. Energy* 224 (C) (Aug. 2018) 550–566.